

Article

Investigation of Mechanical and Thermal Performance of Concrete with *Scallop* Shells as Partial Cement Replacement: Alternative Binder and Life Cycle Assessment

Yassine El Mendili *  and Mohammed-Hichem Benzaama

COMUE Normandie Université—Laboratoire ESITC, 1 Rue Pierre et Marie Curie, 14610 Epron, France

* Correspondence: yassine.el-mendili@esitc-caen.fr; Tel.: +33-231-452-628

Abstract: The adverse environmental impacts of building materials can be achieved by reducing the amount of cement in cementitious composites, specifically when incorporating wastes as partial replacement for Portland cement. In this work, we substitute cement with shell by-products while keeping useful specific properties. *Scallop* shells are good candidates to replace part of the Portland cement as they contain calcium and are available in abundance. We present an experimental and numerical study on the mechanics, hygrothermal behavior, and life cycle analysis of scallop shell concrete. In the fresh state, the replacement of cement by up to 10 wt.% of scallop shells does not significantly affect mortar properties. The results indicate that including 10% shells represents a decrease of up to 40% in the environmental impact, depending on the category of impact considered. Furthermore, the addition of *Scallop* shells makes the material more porous, leading to the facilitation of moisture transfer.

Keywords: alternative binder; *Scallop* shells; microstructural characterization; mechanical and hygrothermal properties; waste valorization; life cycle assessment



Citation: El Mendili, Y.; Benzaama, M.-H. Investigation of Mechanical and Thermal Performance of Concrete with *Scallop* Shells as Partial Cement Replacement: Alternative Binder and Life Cycle Assessment. *CivilEng* **2022**, *3*, 760–778. <https://doi.org/10.3390/civileng3030044>

Academic Editor: Aires Camões

Received: 13 June 2022

Accepted: 19 August 2022

Published: 23 August 2022

Publisher's Note: MDPI stays neutral with regard to jurisdictional claims in published maps and institutional affiliations.



Copyright: © 2022 by the authors. Licensee MDPI, Basel, Switzerland. This article is an open access article distributed under the terms and conditions of the Creative Commons Attribution (CC BY) license (<https://creativecommons.org/licenses/by/4.0/>).

1. Introduction

The reduction of fossil-based energy use continues to be the primary concern in all areas of research in the construction field. In 2017, energy usage in the construction sector accounted for 21% [1] of global total final consumption, ranking third behind the industry and transportation sectors; additionally, 9% [1] of global total final consumption energy was dissipated and never used. All these energy increases raise power production and, as a result, CO₂ emissions.

One of the most recent trends to counter the existing problems of increasing energy use and greenhouse gas emissions is to use low carbon materials, either by enhancing the insulation efficiency of the building structure envelope, and thereby reducing energy consumption, or by developing new low carbon materials.

Low-carbon construction materials are typically bio-based or created by minimizing the quantities of high carbon inputs, with the use of different types of wastes. One of the most available waste products in Normandy (France) is seashells. Indeed, they represent the largest volumes available, and the deposit is of the order of 200,000 tons [2]. The huge quantities of shellfish abandoned on the seashore and in the municipal garbage cans show that their use is not very frequent.

Concretes with partial replacement of cement by seashells can present a good solution to decreasing CO₂ emissions as well as providing adequate mechanical and thermal properties compared to usual concrete [2]. Seashells are composed of at least 95 % of calcium carbonates (CaCO₃), which is comparable to calcium carbonate contents in limestone powders used for Portland cement production [3]. As stated in the literature, the principal component of scallop shells (SS) is calcite (CaCO₃), which can be used as an additional cementitious material. The European standard EN 197-1 states that calcium

carbonate (CaCO_3) or limestone can be incorporated up to 35% in Portland cement. CaCO_3 acts principally as an inert filler when the replacement level is above 5%, due to its low solubility [2].

Studies dealing with the feasibility of using seashells in concrete fabrication have increased in the last decade. The majority of works on shell concrete have been dedicated only to its mechanical behavior, such as Bouasria et al. [2,4], Varhen et al. [5], Neamitha et al. [6].

M. Bouasria et al. [2] used the *Crepidula Forficata* shells (CR) and ferronickel slag (FNS) as a structural component and a partial replacement in mortar. Mortar mixtures using different percentages of FNS and CR shells were formulated and tested up to failure. The results showed that the partial replacement of cement by up to 30% of FNS-CR mix has no significant effect on the workability of the cement in the fresh state. However, with incorporation above 30%, a slight loss of workability was observed. Water absorption by these additives exhibiting high specific surface area is responsible for this loss of workability. The hygrothermal behavior and life cycle analysis (LCA) was not developed in this study.

The absorption and permeability of seashell concrete is rarely reported in previous studies and needs to be further investigated. There are three promising experimental studies in which the authors investigate the potential of cockle shell ash as a material for partial cement replacement [7–9]. Nor Hazurina et al. [7] present the absorption and porosity results of concrete produced with various cockle shell ash replacements in comparison with a standard concrete. It is clearly demonstrated that cockle shell ash reduces the absorption of concrete at low percentages of replacement (below 15%). However, the absorption is increased with increased seashell content (25% and 50%). The absorption and porosity results can be related to the amorphous calcium carbonate nature present in seashell ash [8]. At lower percentages of replacements, the ash particles interlock with each other and fill the gaps in the concrete matrix, which leads to a decrease in the porosity and absorption. However, at higher replacement level, voids are formed due to the aragonite shape of seashell ashes, resulting in higher porosity and absorption [8]. Furthermore, Othman et al. [9] showed that the permeability of the concrete mixtures with cockle shell ash was higher than in the control concrete after 28 days and 90 days of curing. However, at the age of 120 days, the water permeability of the concrete mix with cockle shell ash was lower, except for the 50% replacement ratio. Previous studies have evaluated either the physical and mechanical properties of shell concrete, but none have considered life cycle assessment and hygrothermal behavior both at the same time and at the building scale.

To our knowledge, apart from the few studies presented above, the hygrothermal behavior and life cycle analysis are not well reported on in the literature. S. Cao et al. [10] and S.S. Sui Jiang et al. [11] show the capacity of the Wufi Plus software for the study of the hygrothermal behavior at the building scale. WUFI Plus is an advanced commercial software that helps the user simulate the impact of the energy performance of a building by considering the effects of moisture and heat at the same time [11].

Motivated by these recent results, in this paper we present a hygrothermal and environmental analysis of concrete based on the partial substitution of cement by scallop shells. The life cycle analysis (Using SimaPro and Pleiades tools) and hygrothermal behavior at the building scale (Using Wufi Plus tools) are evaluated. The research questions corresponding to the objectives are:

- What is the environmental effect of shell concrete?
- What is the environmental benefit from the substitution of cement?
- What is the hygrothermal performance of shell concrete at building scale?

The paper is organized as follows: the experimental device and the numerical model are presented in Section 2. Section 3 is dedicated to the analysis of the results and their discussion, followed by the perspectives and conclusions.

2. Materials and Methods

2.1. Methodology

In line with what has been already proposed in the literature, we have developed a new conceptual framework that summarizes and visualizes our research methodology. The conceptual study plan of our work consists of three main parts, as illustrated in Figure 1. Each part is composed of several steps. These will be explained in detail in the following sections.

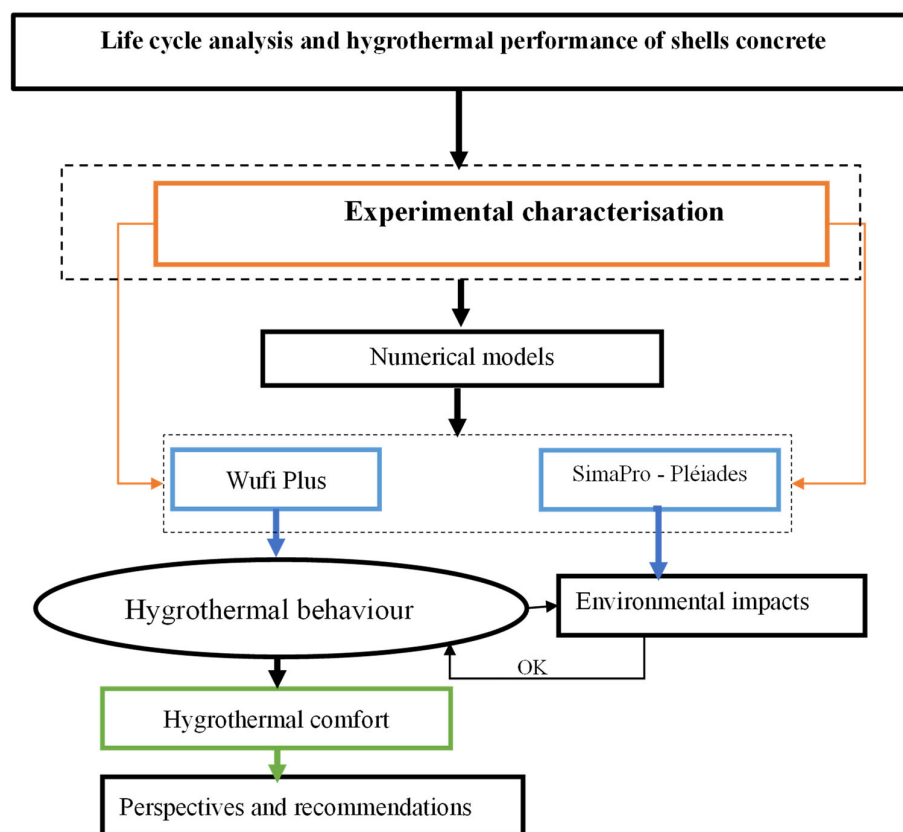


Figure 1. Conceptual study plan.

2.2. Concrete Properties

Mechanical properties are determined on mortars and thermal properties on concretes.

The scallop shell concretes used in this study for thermal measurements are composed of:

- CEM I 52.5 N cement with a density of $3.2 \text{ g}\cdot\text{cm}^{-3}$ and a fineness of Blaine of $4100 \text{ cm}^2\cdot\text{g}^{-1}$. Its d_{10} , d_{50} , and d_{90} were determined using a laser diffraction particle size analyzer and are 2.43, 14.22, and $38.48 \mu\text{m}$, respectively (Figure 2b).
- Standardized sand according to EN 196-1-1.
- Crushed gravel 3/8 mm with a density of $2.65 \text{ g}\cdot\text{cm}^{-3}$ and an absorption coefficient of 0.66%.
- Scallop shells (SS) collected in Ouistreham (Normandy, France), cleaned, crushed, and ground. Before being crushed with a drum compactor, the seashells were washed and dried at $40 \text{ }^\circ\text{C}$ to remove any apparent meat traces and contaminants. The collected seashells aggregates were re-crushed by the Los Angeles abrasion machine and sieved through a $63 \mu\text{m}$ sieve in order to generate scallop seashell powder. The density and Blaine fineness were $2.68 \text{ g}\cdot\text{cm}^{-3}$ and $7890 \text{ cm}^2\cdot\text{g}^{-1}$ respectively. Its d_{10} and d_{90} were determined using a laser diffraction particle size analyzer and are 2.88, 22.78, and $49.48 \mu\text{m}$, respectively (Figure 2a). The d_{50} for the CEM I 52.5 N was $14.22 \mu\text{m}$ and the SS was $22.78 \mu\text{m}$. Cements have finer particle sizes than seashells. Finer size will

offer more specific surface area for an accelerated hydration reaction. The acceleration of the hydration process will result in a rapid development of concrete strength.

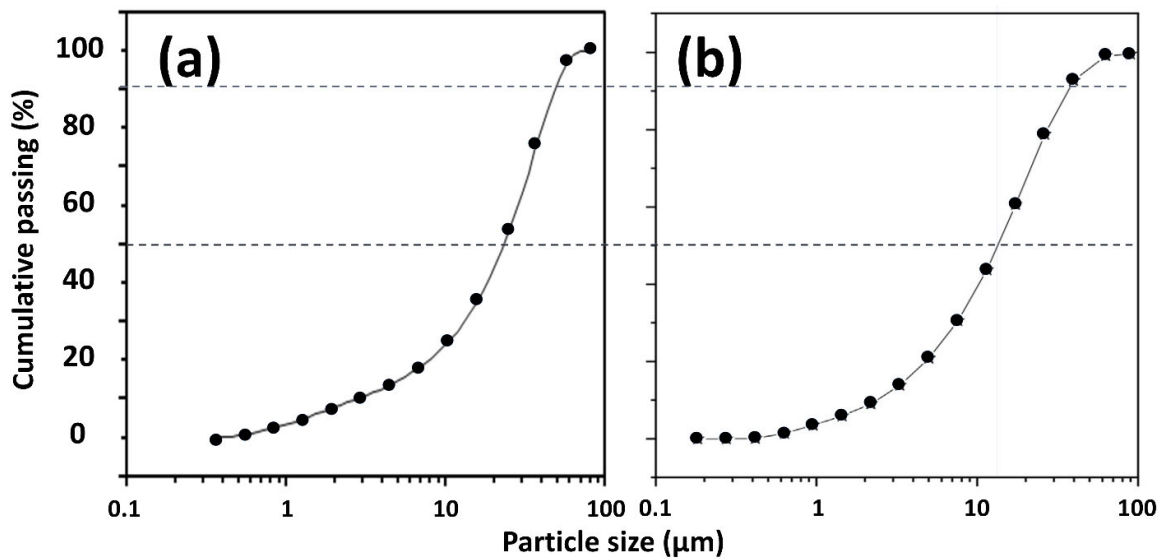


Figure 2. Particle size distribution of (a): Scallop shells and (b): cement used in this study.

Table 1. Calcium is the major element. The analysis also shows the presence of traces of S, Na, Mg, S, and Al (<0.4 wt.%).

Table 1. Chemical composition of SS obtained by energy dispersive spectroscopy on ground SS powders. * O and C are taken with caution as being low precision; d.l.: detection limit.

Element	O *	C *	Ca	Na	S	Mg	Si	Al	Cl	Total
(wt.%)	34.5 ± 2.8	12.6 ± 0.5	51.3 ± 1.6	0.4 ± 0.1	0.4 ± 0.1	0.3 ± 0.1	0.3 ± 0.1	0.2 ± 0.1	d.l.	100

The elaborated concrete specimens are prismatic samples of 30 cm × 30 cm × 7 cm. All specimens were compacted on a vibrating table. The concretes were demolded after 24 h and then placed at 20 °C and 95% relative humidity for 28 days of curing (Figure 3).



Figure 3. Scallop shell concretes prepared for this study.

The mortars were made from CEM I 52.5 N cement and standardized sand. The 4 cm × 4 cm × 16 cm mortars were made with a water/cement ratio set at 0.5 and a

sand/cement ratio set at 3, according to EN 196-1. The samples were placed in a controlled atmosphere (20 ± 1 °C and 90% RH). Cement was replaced by 5 and 10% shell waste (SS).

The composition of the mortar and concrete mixtures is given in Table 2.

Table 2. Composition of the different mortar and concrete mixes ($\text{Kg}\cdot\text{m}^{-3}$).

Mortar	CM	SS5	SS10
Cement	450	428	409
Fine sand 0/3	1350	1350	1350
Scallop shells	0	22	41
Water	225	225	225
Concrete	CC	SS5	SS10
Cement	350	332.5	315
Fine sand 0/3	756	756	756
Gravel 3/8	980	980	980
Scallop shells	0	17.5	35
Water	175	175	175

2.3. Characterization Techniques

X-ray diffraction of the scallop powder was performed at room temperature on a D8 Advance Vario 1 Bruker (two-circle diffractometer, θ - 2θ Bragg-Brentano mode, Cu $K\alpha$ radiation: $\lambda = 1.54059$ Å). The identification was performed using the Crystallography Open Database [12] and quantification was achieved using MAUD software [13].

All Raman spectra presented in this study were recorded at room temperature using a Thermo DXR Raman microscope (Thermo Fisher Scientific Inc., Waltham, MA, USA), with a 532 nm laser as an excitation source used for Vibrational analyses. Raman spectra were recorded at 1 mW and with an integration time of 30 s.

The thermal conductivity was analyzed using a system of Heat Flow meter NETZSCH (Model HFM 436 Lambda). The test sample, with prismatic dimensions of 30 cm \times 30 cm \times 7 cm, is placed between the cooling plate and the heater plate; the heat flows from the heater plate through the sample to the cooling plate from where it is carried off. The cooling and heater plate temperature is adjusted by a Peltier cryostat to establish a temperature gradient from the heater plate across the specimen of $10 \div 30$ °C.

Specific heat capacity (C_p) characterizes the ability of a material to store thermal energy. C_p measurements are performed with a Differential Scanning Calorimetry technique (DSC, NETZSCH STA 449 F3) according to the standard ISO 11357-4. Data are collected from -20 °C to 30 °C continuously with heating rate of 1 °C \cdot min $^{-1}$.

2.4. Test Methods

The specific surface area of each cement mixture used in this study was determined with the Blaine air permeability apparatus according to the ASTM C-204 test method [14].

Workability tests were carried out using a mortar maniabilimeter according to the NF P18-452 standard [15]. The initial and final setting time for all mixtures was measured according to the NF P 15-431 standard [16]. The compressive and three-point bending tests were conducted according to the EN 196-1 standard [17].

2.5. Model of Heat and Moisture Transfer in Building Envelopes

WUFI-PLUS is used to simulate the thermal and moisture behavior of the building and the moisture flow into the room through the envelope structure. It is the most complete heat and moisture simulation tool in the WUFI[®] software family [18]. In addition to simulating hygrothermal conditions in building components, WUFI[®] Plus simulates the indoor environment and is therefore suitable for addressing comfort and energy consumption in

buildings [18]. Simulation of the interaction between building usage and system technology allows for integral assessment of indoor climate, hygienic conditions, thermal comfort, indoor air quality, and damage to components as a function of heating and cooling loads, and the necessary effort to humidify/dehumidify [18]. The indoor air heat and moisture balance equations in Wufi Plus are as follows:

- Heat balance Equation:

$$\rho C_p V \frac{\partial T(\tau)}{\partial \tau} = Q_{e(\tau)} + Q_{e(\tau)} + Q_{v(\tau)} + Q_{s(\tau)} + Q_{f(\tau)} + Q_{HVAC(\tau)} \quad (1)$$

where: $Q_{in(\tau)}$ amount of heat dissipation from the indoor heat source (W), $Q_{e(\tau)}$ convective heat transfer between the inner surface of the envelope and the indoor air (W), $Q_{V(\tau)}$ heat that enters the room (W), $Q_{s(\tau)}$ heat generated by the solar radiation entering the room through the door and window (W), $Q_{f(\tau)}$ heat that the door and window infiltrate into the room (W) $Q_{HVAC(\tau)}$ heat supply or cooling capacity of the air conditioner (W).

- Moisture equilibrium Equation:

$$\rho C_p V \frac{\partial W(\tau)}{\partial \tau} = W_{in(\tau)} + W_{e(\tau)} + W_{v(\tau)} + W_{f(\tau)} + W_{HVAC(\tau)} \quad (2)$$

where: $W(\tau)$ indoor air moisture content (kg/kg), $W_{in(\tau)}$ indoor wet source moisture content (kg/s), $W_{e(\tau)}$ amount of moisture exchange between the inner surface of the enclosure structure and the indoor air (kg/s), $W_{V(\tau)}$ amount of moisture entering the room (kg/s), $W_{f(\tau)}$ amount of moisture that the door and window infiltrate into the room (kg/s), $W_{HVAC(\tau)}$ air conditioning humidification (kg/s).

To simulate the hygrothermal performance of the shell concrete, a simplified one-story office building was modelled as shown in Figure 4. The building has a floor area of 79 m² and a total height of 3.6 m with two uncoated double-glazed windows located at the south façade of the structure. The composition of the walls, roof, and slab are presented in the Tables 3 and 4. This composition corresponds to the composition of a BBC building that exists in the Pleiades library. Ordinary concrete will be replaced by shells concrete.

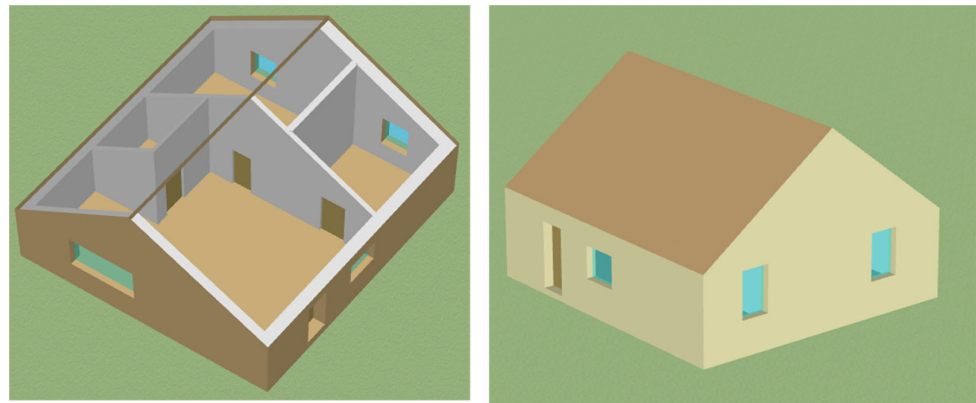


Figure 4. Simulated structure.

The initial conditions used for the Wufi simulation are presented in the table below.

The simulation has been tested for the climatic conditions of the city of Trappes (France) located in zone H1a, as shown Figure 5. In this zone, the maximum temperature difference is 4.82 °C for a winter day. On other hand, the maximum temperature difference is 2.7 °C for a summer day, with maximum energy demand of 60 kWh/m²/year.

2.6. Life Cycle Assessment

The goal of life cycle assessment (LCA) is to determine how damaging items are to the environment, to lessen those effects, and select goods that are least hazardous to the environment. The complete and all-encompassing evaluation of the LCA allows for

ensuring that the environmental effects brought on by potential adjustments to the building product can be compared for various scenarios, and that they are reflected in pertinent decision-making processes. For this reason, the environmental impacts of the developed material were assessed.

Table 3. The composition of the walls, roof, and slab.

Composition	Thickness (m)	Conductivity (W/m·K)	Density (kg/m ³)	Thermal Resistance (m ² K W ⁻¹)
Vertical walls				
Glass wool	0.2	0.041	2	4.88
Concrete	0.2	1.95	460	0.11
Ceiling				
Glass wool	0.26	0.041	3	6.34
Plaster gypsum	0.01	0.42	12	0.02
Slab				
Glass wool	0.2	0.041	2	4.88
Concrete	0.2	1.95	460	0.11

Table 4. Hygrothermal proprieties of seashell concrete.

Concrete	Dry Density	Porosity	Thermal Conductivity	Specific Heat Capacity	Water Vapor Permeability
	kg/m ³	%	W/(m·K)	J/(kg·K)	Kg/(m·s· Pa)
Shells concrete	2250	25 %	1.78	920	2.12×10^{-12}

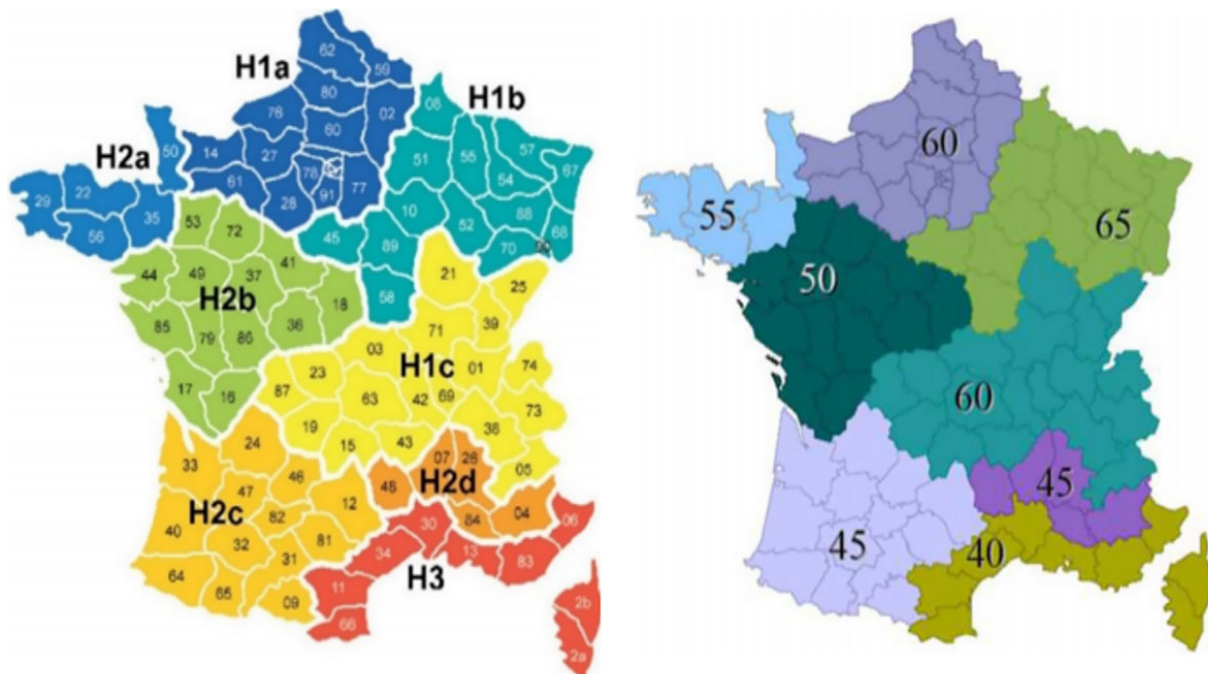


Figure 5. Map of climatic zones and Maximal energy demand [19].

An LCA approach was applied, according to the international standards of the ISO 14040 series, consisting of the following steps: (1) definition of goal and scope; (2) inventory analysis; (3) impact analysis; (4) interpretation (Figure 6).

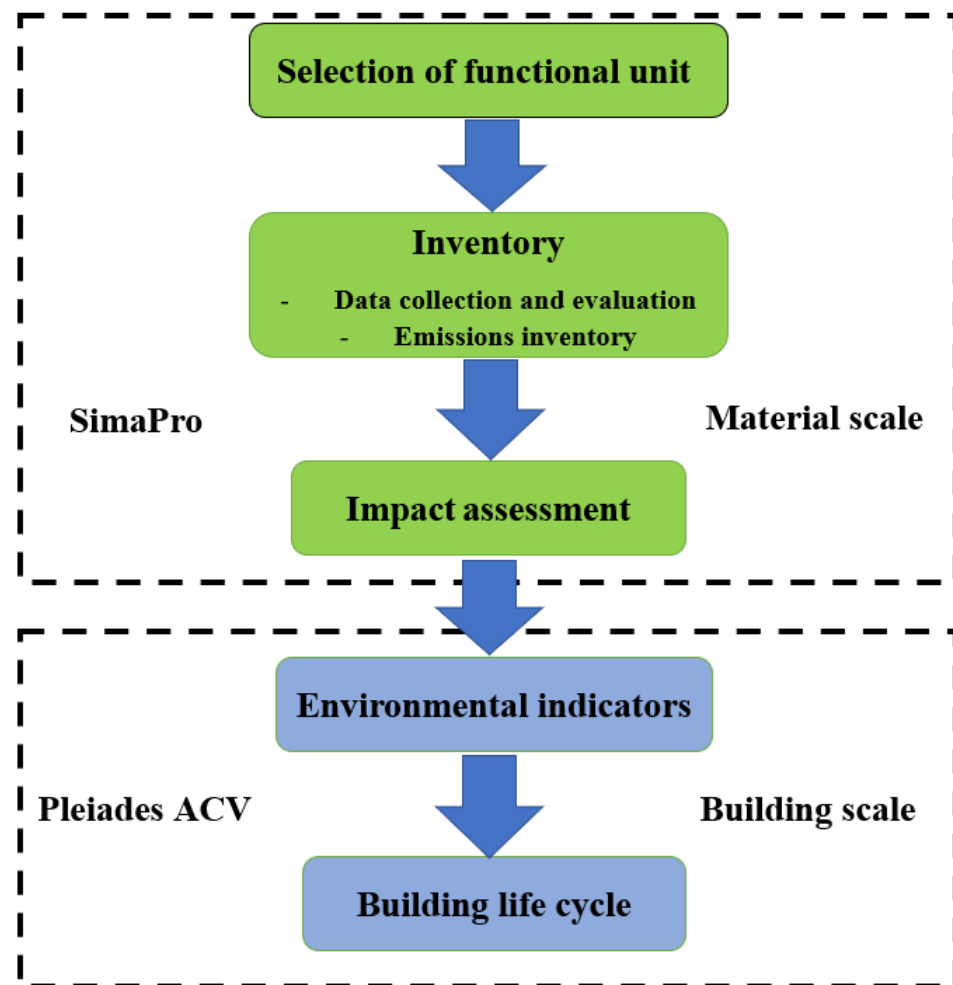


Figure 6. Steps in the LCA process.

The primary objective of this study was to determine and evaluate the environmental impacts of the shell concrete at the material scale using SimaPro tools. According to the ISO 14,040 standard, a reference functional unit must be defined for properly quantifying the environmental performance of the system. The functional unit of the present LCA study was defined to ensure the function of 1 m² for a reference life of 50 years.

For the inventory analysis, the data used in this study was gathered from several sources. Where available and applicable, the Econivent database was used. For the rest of the data, similar studies, reports, or personal communications (laboratory) were used and summarized below. The production of calcium carbonate (CaCO₃) from shells is taken from the study [20] (Table 5). The environmental indicators of calcium carbonate (CaCO₃) are used to perform a life cycle assessment at the building level using Pleiades tools. The building is occupied by four persons and heated by a gas boiler for heating.

Table 5. Inventory: Production of calcium carbonate from shells [20].

Calcium Carbonate	
Shells	100 t
Biocide	0.7 kg
Diesel	57 kg
Water	95 t
Electricity	1.6 E4 kWh
Transport	30 Tkm
Air emissions	
Water	35 m ³
Ammonia	0.2 kg
Particulates < 10 um	0.6 kg
Sulfur dioxide	3 kg
Nitrogen oxides	32.3 kg
Carbon dioxide	1.12 kg
Water emissions	
COD, Chemical Oxygen Demand	8.8 kg
BOD5, Biological Oxygen Demand	0.2 kg
Suspended solids, unspecified	1.6 kg
Nitrogen, organic bound	0.5 kg
Ammonia, as N	0.1 kg
Phosphate	0.1 kg
Nitrate	0.3 kg
End-of-life treatment of concrete: Concrete recycling, crushing (1 kg)	
Diesel combustion	0.0143 MJ
Electricity	0.00398 kWh
Heat (other than natural gas)	0.00491 MJ

3. Results and Discussion

3.1. Experimental Results

3.1.1. XRD Analysis of Scallop Powder

An XRD pattern of the scallop powder can reasonably be refined using calcite structure (Figure 7 and Table 6). The agreement factors Rwp and RB are 9.5% and 7.4%, respectively. This shows the goodness of our fit (GoF = 1.64).

Table 6. Refined values of lattice parameters, unit cell volume, average diameter, microstrain $\langle \epsilon^2 \rangle^{1/2}$. Standard deviations are indicated in parenthesis on the last digit.

Phase	COD Reference	Lattice Type + Space Group	Lattice Parameters (Å)	$\langle D \rangle$ (nm)	$\langle \epsilon^2 \rangle^{1/2}$
Calcite (CaCO ₃)	1,547,347	Trigonal R-3c:H	a = 4.986 (1) c = 17.070 (2)	750 (20)	1.10 ⁻³

3.1.2. Permeability of Mix

The addition of SS as a cement substitute slightly reduces the apparent permeability of mortar. The reduction of penetration resistance is mainly attributed to the degeneration of the pore structure. When the pore structure is finer, the penetration resistance is

improved [21]. By adding SS with high fineness, the pore structure is refined and thus the penetration resistance is enhanced (Table 7).

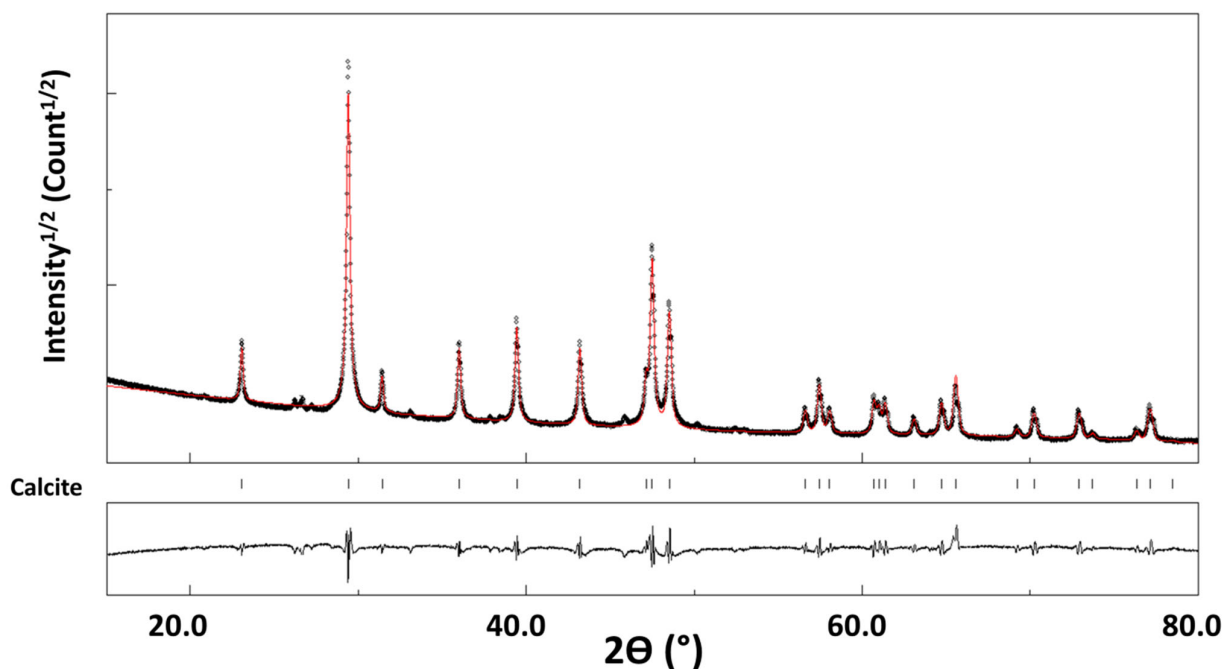


Figure 7. X-ray diffraction pattern of scallop powder refined with the MAUD software.

Table 7. Mortar composition and permeability after 28 days.

Sample	Mass Substitution Rate of Cement by SS (%)	Permeability after 28 Days ($\text{m}\cdot\text{s}^{-1}$)
CM	0	2.80×10^{-12}
SS5	5	2.12×10^{-12}
SS10	10	1.87×10^{-12}

3.1.3. Mortar Densities and SSA

For all mortars, an increase in the bulk density is observed with increases in the curing time from 2 up to 28 days (Figure 8a). Increasing the SS proportion led to a gradual decrease in mortar density at all curing times. This decrease is attributed to the low density of SS compared to that of the used cement. As seen in Figure 8a, the decrease is more accentuated after 2 days then after 28 days. This is due to a further densification and porosity decreases with time.

The addition of SS increases the specific surface area (SSA) of the cement powder (Figure 8b). This reduction is attributed to a larger Blaine specific surface area of SS compared to that of cement ($4100 \text{ cm}^2/\text{g}$).

- Fresh state mortar properties

Our analysis shows that the substitution of cement by SS has no effect on the flow times. Indeed, all mixes present a good flow time with values close to 7 s. The water content required for the normal consistency of paste is similar for the CM and M-SS5 and decreased slightly with the incorporation of 10% of SS (Figure 9a). However, the water requirements of SS cement are comparable to those of conventional supplementary cementitious materials, such as pozzolana, fly ash, and slag [22].

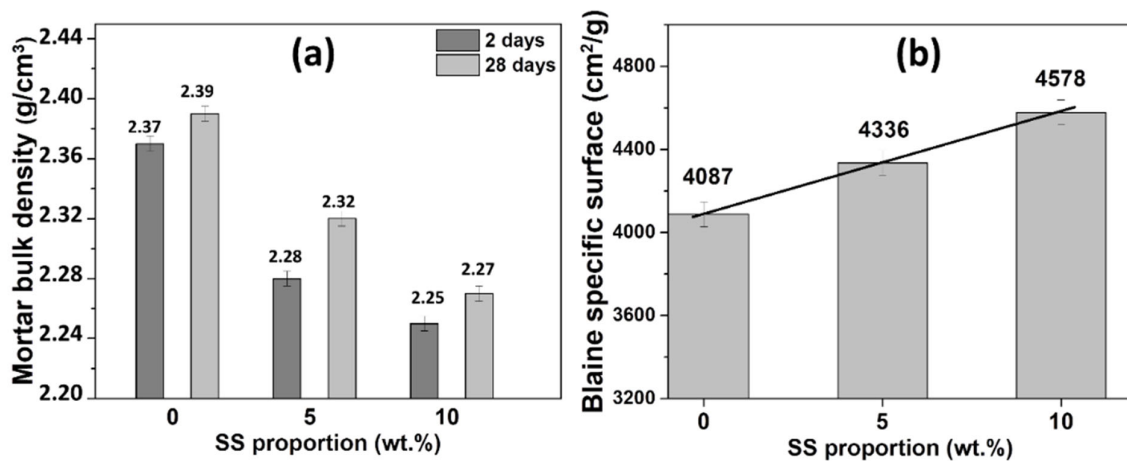


Figure 8. Evolution of: (a) the density and (b) Blaine specific surface area (SSA) of the cements elaborated with different proportions of SS.

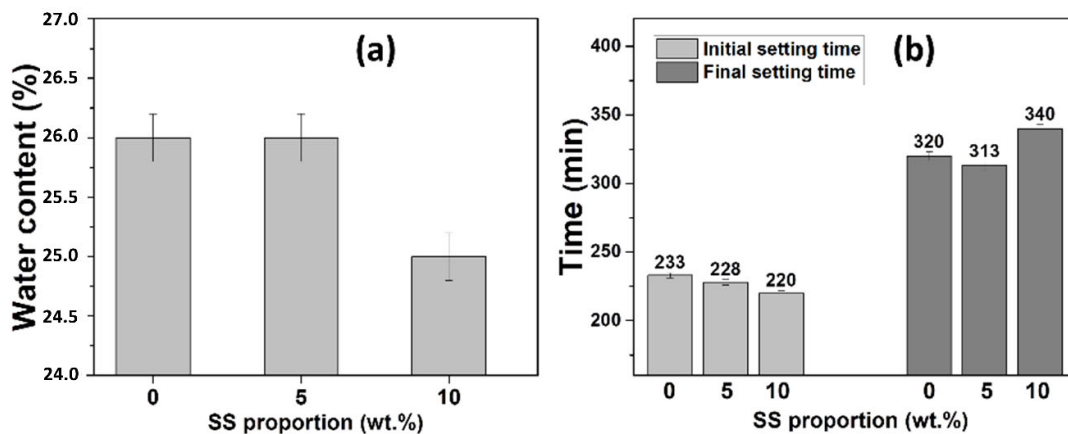


Figure 9. (a) Flow time and (b) SS mortars setting time.

The evolution of initial and final setting time of cement pastes with the SS ratio increase is presented in Figure 9b. The values of setting times of all paste mixes are in accordance with the NF P 15-431 standard [16]. The results show that the increase of the SS content up to 10% slightly reduced the initial setting times compared to the control paste. At the cement substitution ratio of 5%, the SS decreased the initial and final setting time by 5 min and 8 min, respectively in comparison to those of the control paste. At the cement substitution ratio of 10%, the SS decreased the initial setting time by 5 min, but the final setting time increased slightly, by 20 min. The decrease in setting time is expected and is probably due to the high finesses of SS particles, which leads to a significant increase in the number of nucleation sites, favoring the formation of more hydration products, and thus accelerating the hydration reactions [23,24]. However, an increase in the SS rate below 10% of the cement will increase the separation distance between hydrated cement particles, retard the formation of capillary bridges, and delay the formation of an interlocking network between the particles [25].

- Compressive and flexural strength of mortar

The compressive and flexural strength values of elaborated mortars after 2, 7, 14, and 28 curing days are presented in Figure 10. Regardless of the considered formulation, the mortar's compressive strength increases with time. The results show also that only the 5% cement replacement by SS produced higher strength for all curing times. Indeed, the compressive and flexural strengths for the M-SS5 mortar increase, and surpass the control mortar at 28 days, by 6.6%. The maximum compressive strength at 28 days is

then obtained with 5% SS replacement with a value of 60.45 MPa. Above 10% of SS substitution, the compressive strength decreases with the replacement rate and is greater than 50 MPa. However, the results obtained for the cement mortar mixes with 10% of SS are still acceptable for application in the construction industry.

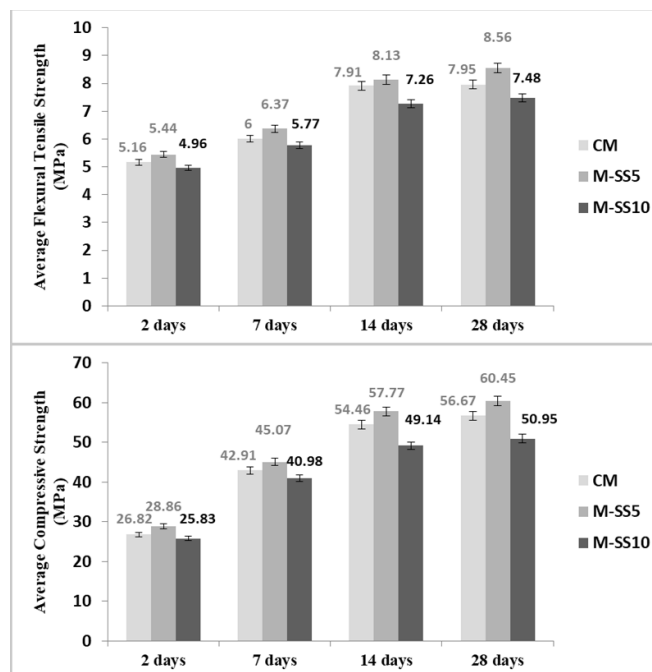


Figure 10. Average compressive and flexural tensile strengths at different ages of the mixtures with SS additions.

Generally, only certain mixtures with calcium carbonates systems (such as limestone and SS) resulted in high compressive strength compared to the CM. The decrease in strength at high levels of replacement is probably due to the high finesses of SS compared to cement, and the subsequent aggregation of SS particles at high proportions. The aggregation of SS particles will destabilize the system by preventing the formation of homogeneous hydrated microstructures, and thus leading to a strength decrease [26].

If the content of shells and the distance between the SS particles are appropriate, the CSH hydration will be suitably controlled, limiting the growth of portlandite. In addition, the high fineness of SS particles in mortar promotes the hydration of cement due to their high activity and the dissolution of calcium present at high proportions.

After 28 days of age, Raman examinations of the control mortar surface (Figure 11) reveal the presence of C-S-H.

There has been extensive research on the Raman spectra of the C-S-H systems [27,28]. Si-O stretching is responsible for the band with the highest intensity at 680 cm^{-1} . A contribution at 445 cm^{-1} is attributed to the twisting and stretching of the Si-O-Si bounds, and bands in the range of $950\text{ to }1100\text{ cm}^{-1}$ are connected to the symmetric stretching modes of Q_n species in silicates (Si-O). These bands are present in the low wavenumber range ($100\text{--}360\text{ cm}^{-1}$) and are attributed to the lattice vibrations of Ca O polyhedra. When the Raman spectra of C-S-H formed on non-substituted mortars and SS5-SS10 are compared, there is a significant increase in intensity and decrease in bandwidths of the vibrational modes (lattice vibrations of Ca-O polyhedral) as a function of seashell content increase. This phenomenon is due to the addition of scallop shells, which lead to an increase in the ordering of the calcium environment, resulting in a higher degree of polymerization.

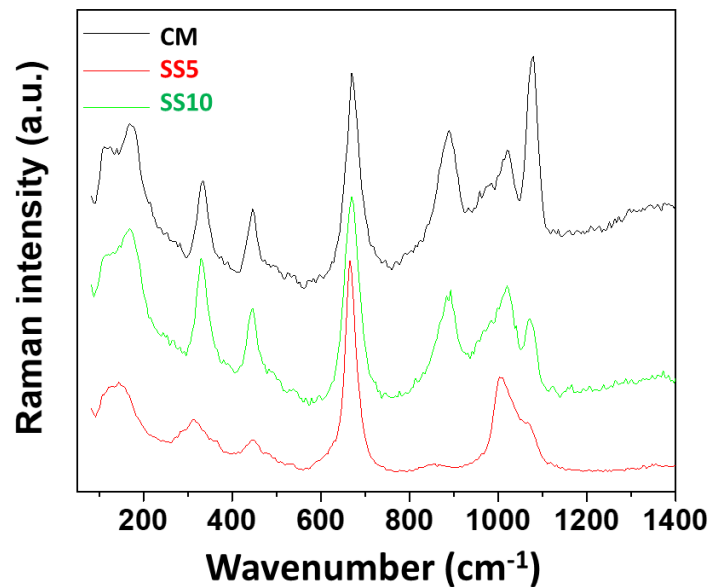


Figure 11. Raman spectra of the mortar surfaces after 28 days of curing.

For the specimen with seashell, ettringite produced by the C3S hydration of cement is also formed, in addition to C-S-H. Calcite can be found in all mortar samples (not shown here). The release of Ca^{2+} and CO_3^{2-} ions occurs after the dissolution of calcite originating from seashells. The dissolved CO_3^{2-} ions can also participate in hydration processes, particularly those involving the aluminate phases, resulting in the development of carboaluminate hydrates instead of sulfoaluminate hydrates, stabilizing the ettringite developed at young ages [2].

Several studies have examined the use of shells as partial substitute in cement [2,3,29]. The amounts of ettringite and calcium carboaluminate in the mixtures increased as the amount of shell powder increased. This explains how shell powder can promote the precipitation of hydration products (C-S-H). The effectiveness of seashells was attributed to the liberation of CO_3^{2-} ions, which led to the formation of carboaluminates and the reduction of concrete porosity, which increased flexural and compressive strengths. Wang et al. demonstrated that the water absorption of concrete increases with CaCO_3 content, and that concrete with a higher cockle shell ash content is more porous [30].

- Thermal conductivity of seashell concrete

As can be seen from Table 8, thermal conductivity of the formulated control concrete is $1.95 \text{ W}\cdot\text{m}^{-1}\cdot\text{K}^{-1}$. For the specimen M-SS10, the value of thermal conductivity is $1.78 \text{ W}\cdot\text{m}^{-1}\cdot\text{K}^{-1}$. These results show that the addition of SS slightly improves the thermal conductivity of the concrete. Indeed, the use of 10% of SS decreased the thermal conductivity by 9% at 20°C in comparison with standard concrete.

Table 8. Variation of the thermal conductivity, porosity, and density of the concretes elaborated with different proportions of SS after 28 days of curing. Standard deviations are calculated for 3 replicates.

Sample	Porosity	Density ($\text{g}\cdot\text{cm}^{-3}$)	Thermal Conductivity ($\text{W}\cdot\text{m}^{-1}\cdot\text{K}^{-1}$)
CM	32%	2.37 ± 0.5	1.95 ± 0.03
SS5	28%	2.28 ± 0.5	1.86 ± 0.02
SS10	25%	2.25 ± 0.5	1.78 ± 0.02

- Life cycle analysis

The environmental impact results of shell concrete production are presented in Figure 9 for 1 m^2 using SimaPro tools. The impact results are presented as a percentage of the

greatest impact in each category. The results show that the cement and sand materials stand out as the largest contributors to the environmental impacts. For 10% of cement substitution by shells, cement has an impact of 80% for the indicator “Climate change” (Figure 12a). Furthermore, the shells generate a maximum rate of 41% for the indicator “Marine eutrophication”. This seems to indicate that including 10% shells represents a decrease of up to 40% of the environmental impact, depending on the category of impact considered (Figure 12b).

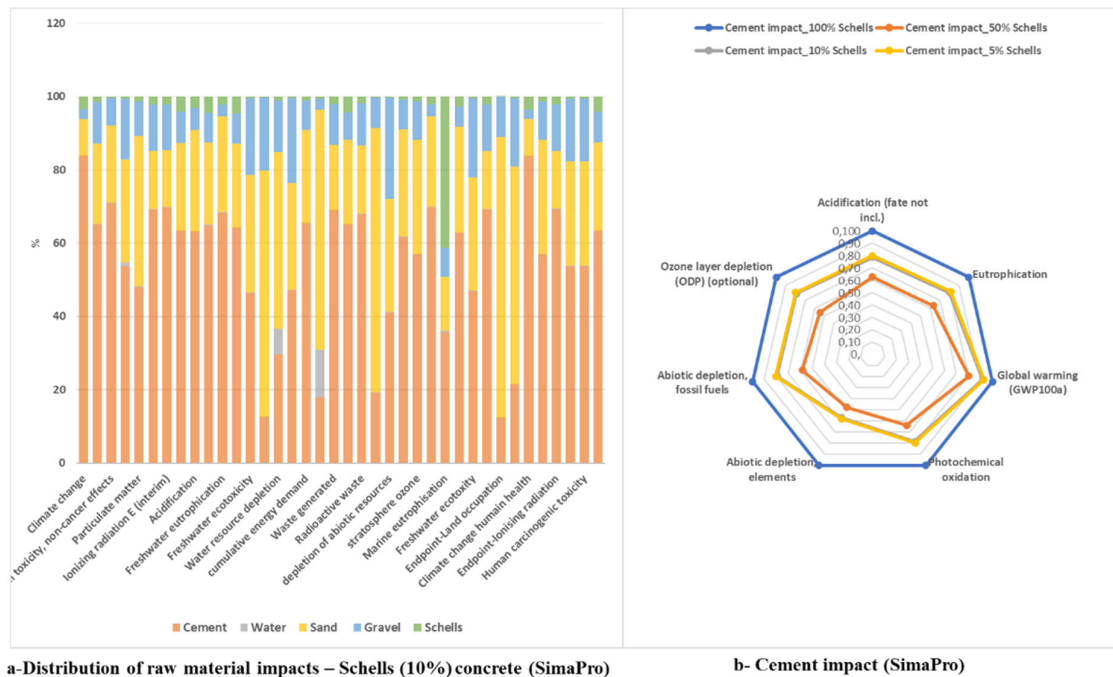


Figure 12. Environmental impact. (a) Distribution of raw material impacts and (b) Cement impact.

To identify the elements of the life cycle of a building (Figure 3) based on shell concrete (10%), a contribution analysis has been carried out using Pleiades software, as shown Figure 13. This analysis focuses on 33 impact indicators representative of the sum of the four phases of a building’s life cycle (construction, use, renovation, and demolition). The simulation was made for a life cycle based on four occupants. The results show that the construction and renovation phases are the most important. This finding confirms the results obtained by Lotteau et al. [31] who showed that the utilization phase of the building produces the most important environmental impacts in terms of quantity.

Therefore, we focused particularly on the greenhouse effect, as shown Figure 14. Given the importance of the use and retrofit phases, it is interesting to determine which assumptions lead to this difference. The results show that the heating is the most impactful element. The use of a gas boiler has a significant impact on the environment, because of its lifespan, and has a very important impact on all the indicators. It is considered that DHW (Domestic Hot Water) tanks and HVAC systems (Heating, Ventilation, and Air-Conditioning) should be replaced every 20 years. The renovation phase consists mainly of the renewal of windows and internal walls.

- Hygrothermal behavior

The building is located in Trappes, France, which has a humid climate with mean values of temperature and humidity of 14 °C and 75%, respectively. The weather data used in this work was obtained from the database embedded in the WUFI® Plus program, which is shown in Figure 15.

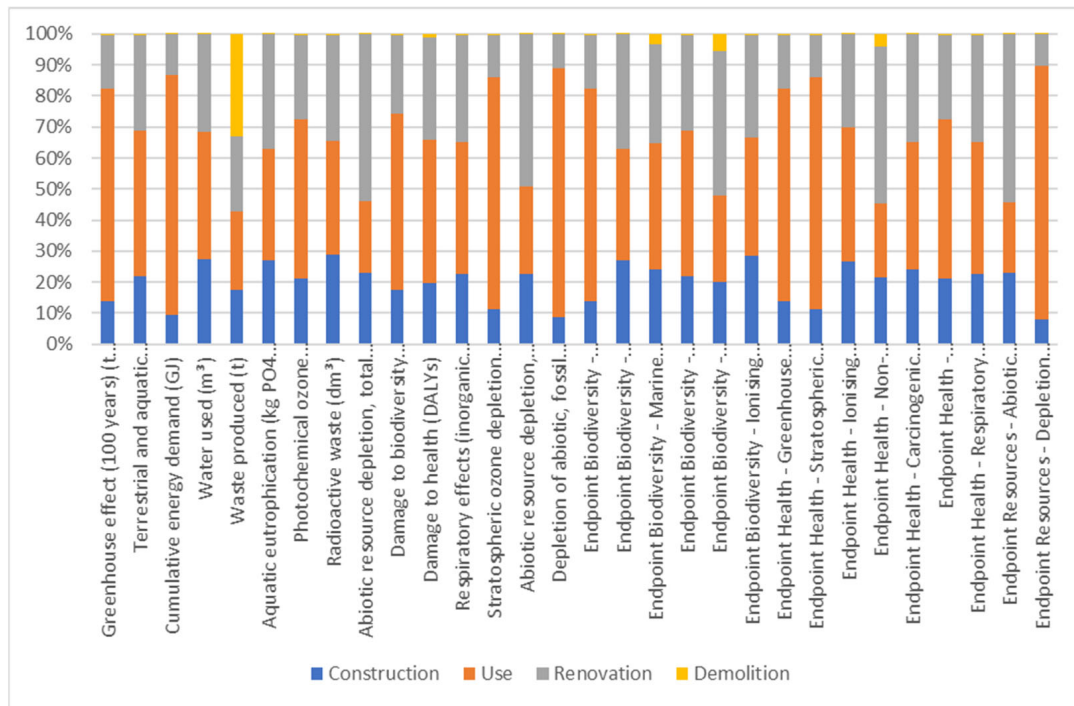


Figure 13. Impacts distribution according to life stage.

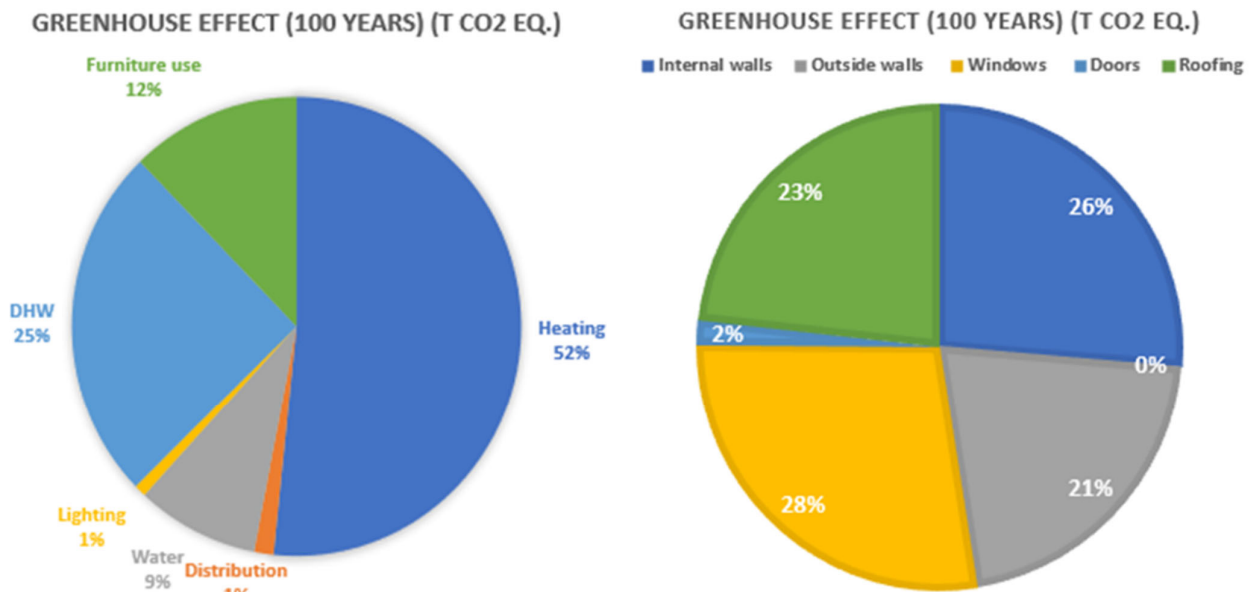


Figure 14. Greenhouse effect for the use and retrofit phases.

For the simulation, it is assumed that the building has four occupants. In this study we are interested in hygrothermal comfort, as shown in Figure 16, without mechanical cooling/heating systems. As shown in Figure 16a, a high indoor relative humidity has been observed which can negatively influence human health. For some time periods, the optimal thermal comfort was not ensured, and circles move outside of the optimal thermal comfort region due to the higher relative humidity. A good level of comfort can also be found in other periods. The variation of humidity inside the building is influenced by the occupants and the porosity of the wall. For this purpose, in Figure 16b we present the variation of inner moisture source (occupants) and moisture exchange with partitions. The results in Figure 16b show that the wall can provide, or release moisture generated by

the occupants. Positive values represent moisture added to the zone and negative values represent moisture leaving the zone.

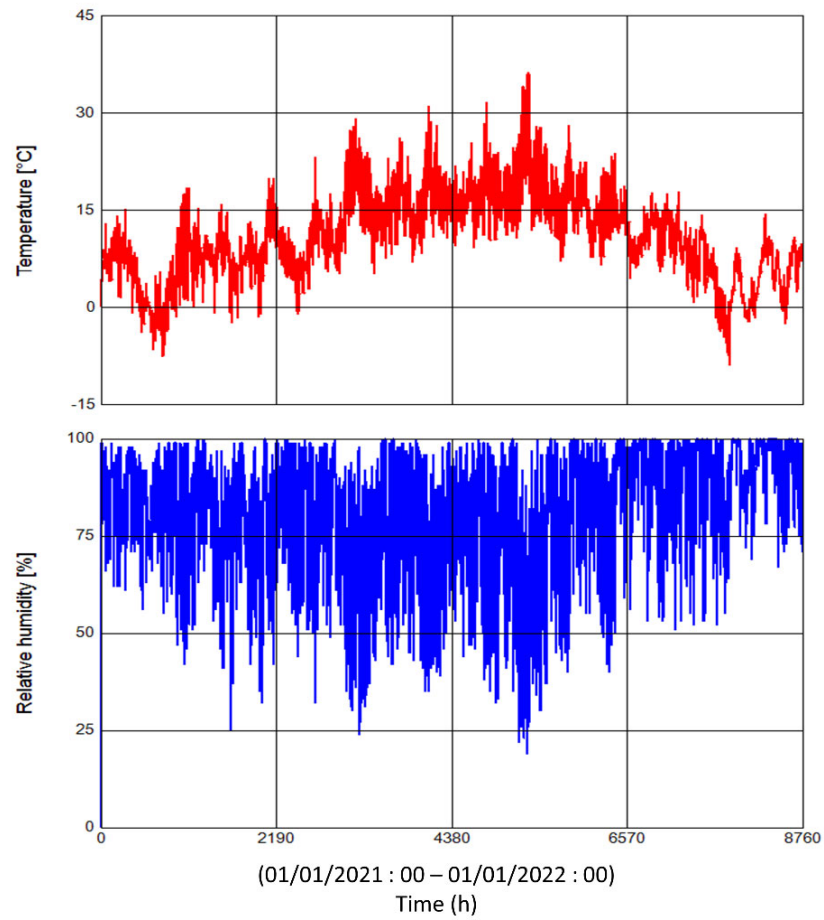


Figure 15. Climatic conditions.

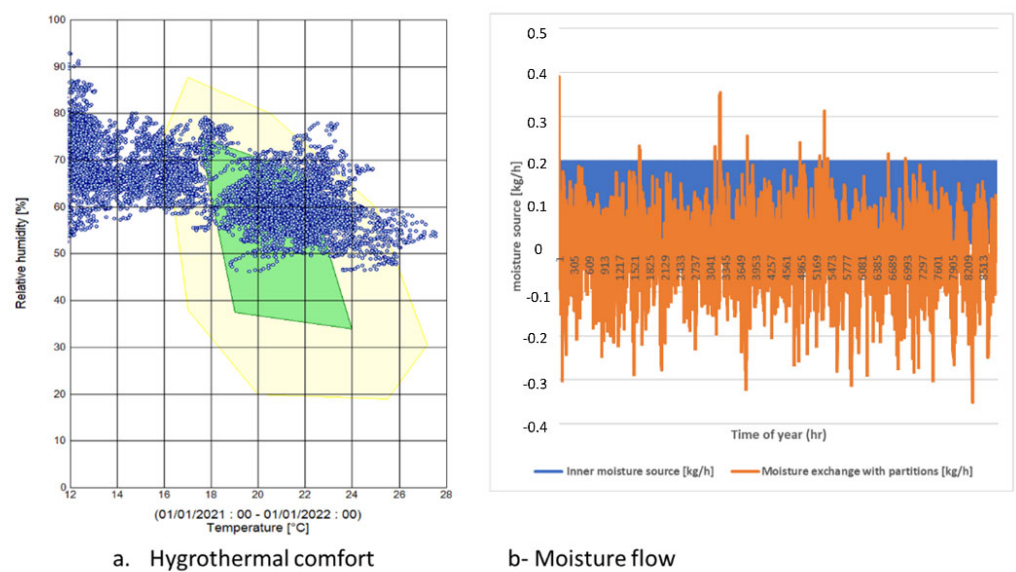


Figure 16. (a) Hygrothermal comfort and (b) moisture flow.

4. Conclusions

This paper presents the effects of cement substitution by scallop shells at different levels. The hygrothermal and mechanical characterizations of the scallop shell concrete sample as well as the numerical analysis accompanied by LCA yield some promising findings, which may be summarized as follows:

- The replacement of cement by up to 10 wt.% of scallop shells does not significantly affect mortar properties.
- The greater effectiveness of scallop shells is attributed to their higher calcium content and the high finesses of SS particles in mortar, which promote the hydration of cement due to their high activity and the dissolution of calcium present at high proportion in scallop shells.
- A real potential for the use of scallop shells by-products as partial replacement for cement, at an optimum rate of 10% is evidenced.
- This new material is a good candidate to extensively contribute to the achievement of sustainable development goals and carbon emission reduction. Indeed, the results indicate that cement substitution by 10% shells in concrete represents a decrease up to 40% of the environmental impact.
- The results found using Wufi, show that the wall ensures a hygroscopic exchange which allows the evacuation of the humidity generated by the occupants.

These initial findings highlight the need for further complementary investigations. Indeed, this work presents some limitations:

- With regard to thermal properties, thermal conductivity and thermal diffusivity has been studied; nevertheless, mass loss via a differential scanning calorimeter and thermo-gravimetric analysis is necessary to determine selected characteristics of materials that exhibit either mass loss or gain due to decomposition or oxidation. XRD analysis will also be necessary to understand the effect of the addition of carbonates on the mineralogical composition of the concrete, and thus to understand the hydration mechanism of the cement.
- The shear behavior here is one of the properties to be studied in the future as fracture in a material is often due to shear.

Author Contributions: Conceptualization, Y.E.M. and M.-H.B., methodology, Y.E.M. and M.-H.B., software, Y.E.M. and M.-H.B., validation, Y.E.M. and M.-H.B., analysis Y.E.M. and M.-H.B., investigation, Y.E.M. and M.-H.B., data curation, Y.E.M. and M.-H.B., writing—original draft preparation, Y.E.M. and M.-H.B., writing—review and editing, Y.E.M. and M.-H.B., visualization, Y.E.M. and M.-H.B. All authors have read and agreed to the published version of the manuscript.

Funding: This research is supported by the European Regional Development Fund for having sponsored this study within the framework of a BLUEPRINT to a Circular Economy project (Interreg V A France (Channel) England, Project n°206).

Institutional Review Board Statement: Not applicable.

Informed Consent Statement: Not applicable.

Data Availability Statement: Not applicable.

Acknowledgments: This research is associated with the national DD&RS strategy (Sustainable Development and Social Responsibility, ‘développement durable et responsabilité sociale’ in French).

Conflicts of Interest: The authors declare no conflict of interest.

References

1. United Nations et Department of Economic and Social Affairs, Energy Statistics Pocketbook, United Nation, OSBN-10 9212591485, San Fransisco, CA, USA. 2020. Available online: <https://unstats.un.org/unsd/energystats/pubs/documents/2020pb-web.pdf> (accessed on 12 June 2022).
2. Bouasria, M.; Khadraoui, F.; Benzaama, M.-H.; Touati, K.; Chateigner, D.; Gascoin, S.; Pralong, V.; Orberger, B.; Babouri, L.; Mendili, Y.E. Partial substitution of cement by the association of Ferronickel slags and *Crepidula fornicata* shells. *J. Build. Eng.* **2021**, *33*, 101587. [CrossRef]
3. Mosher, S.; Cope, G.W.; Weber, F.X.; Shea, D.; Kwak, T.J. Effects of lead on Na⁺, K⁺-ATPase and hemolymph ion concentrations in the freshwater mussel *Elliptio complanate*. *Environ. Toxicol.* **2012**, *27*, 268–276. [CrossRef] [PubMed]
4. Bouasria, M.; Benzaama, M.H.; Pralong, V.; El Mendili, Y. Mechanical and hygrothermal performance of fly-ash and seashells concrete: In situ experimental study and smart hygrothermal modeling for Normandy climate conditions. *Archives. Civil. Mechan. Eng.* **2022**, *22*, 100. [CrossRef]
5. Varhen, C.; Carrillo, S.; Ruiz, G. Experimental investigation of peruvian scallop used as fine aggregate in concrete. *Constr. Build. Mater.* **2017**, *136*, 533–540. [CrossRef]
6. Neamitha, M.; Muthadhi, A. Performance of pervious concrete with industrial waste as coarse aggregate e an overview. *Int. J. Emerg. Technol. Adv. Eng.* **2016**, *6*, 155–161.
7. Nor Hazurina, O.A.B.; Megat Johari, B.H.; MA Mat Don, M. Potential use of cockle (*anadara granosa*) shell ash as partial cement replacement in concrete. *Casp. J. Appl. Sci. Res.* **2013**, *2*, 369–376.
8. Bassam, A.T.; Mohammed, W.H.; Zeyad, A.M.; Yusuf, M.O. Properties of concrete containing recycled seashells as cement partial replacement: A review. *J. Clean. Prod.* **2019**, *237*, 117723.
9. Othman, N.H.; Bakar, B.H.A.; Don, M.; Johari, M. Cockle shell ash replacement for cement and filler in concrete. *Malays. J. Civil. Eng.* **2013**, *25*, 201–211. [CrossRef]
10. Cao, S.; Li, X.; Yang, B. Heat and moisture transfer of building envelopes under dynamic and steady-state operation mode of indoor air conditioning. *J. Build. Eng.* **2021**, *44*, 102683. [CrossRef]
11. Jiang, S.S.S.; Hao, J.L.; de Carli, J.N. Hygrothermal and mechanical performance of sustainable concrete: A simulated comparison of mix designs. *J. Build. Eng.* **2021**, *34*, 101859. [CrossRef]
12. Grazulis, S.; Daškevič, A.; Merkys, A.; Chateigner, D.; Lutterotti, L.; Quirós, M.; Serebryanaya, N.R.; Moeck, P.; Downs, R.T.; Le Bail, A. Crystallography Open Database (COD): An open-access collection of crystal structures and platform for world-wide collaboration. *Nucleic. Acids. Res.* **2012**, *40*, D420–D427. [CrossRef] [PubMed]
13. Lutterotti, L.; Matthies, S.; Wenk, H.R.; Schultz, A.S.; Richardson, J.W. Combined texture and structure analysis of deformed limestone from time-of-flight neutron diffraction spectra. *J. Appl. Phys.* **1997**, *81*, 594–600. [CrossRef]
14. ASTM C204-18e1; Standard Test Methods for Fineness of Hydraulic Cement by Air-Permeability Apparatus. ASTM International: West Conshohocken, PA, USA, 2018.
15. NF P18-452, February 2017; Concretes-Measuring the flow time of concretes and mortars using a workabilitymeter. AFNOR: Paris, France, 2017.
16. NF P 15-431. Février 1994. P 15-431; Liants Hydrauliques-Technique Des Essais-Determination Du Temps De Prise Sur Mortier Normal. AFNOR: Paris, France, 1994.
17. NF EN 196-1; Méthodes D'essais Des Ciments-Partie 1: Détermination Des Resistances-Methodes D'essais Des Ciments. AFNOR: Paris, France, 2016.
18. Wuffi, Fraunhofer, Munich, Germany. Available online: <https://wufi.de/en/software/wufi-plus/> (accessed on 12 June 2022).
19. Gounni, A.; Louahlia, H. Dynamic behavior and economic analysis of sustainable building integrating cob and phase change materials. *Constr. Build. Mater.* **2020**, *262*, 120795. [CrossRef]
20. Iribarren, D.; Moreira, M.T.; Feijoo, G. Implementing by-product management into the Life Cycle Assessment of the mussel sector. *Resour. Conserv. Recycl.* **2010**, *54*, 1219–1230. [CrossRef]
21. Zhang, M.H.; Li, H. Pore structure and chloride permeability of concrete containing nano-particles for pavement. *Constr. Build. Mater.* **2011**, *25*, 608–616. [CrossRef]
22. Sobolev, K.; Kozhukhova, M.; Sideris, K.; Menéndez, E.; Santhanam, M. *Properties of Fresh and Hardened Concrete Containing Supplementary Cementitious Materials: State-of-the-Art Report of the RILEM Technical Committee 238-SCM Working Group 4; Alternative Supplementary Cementitious Materials*; Springer International Publishing: Cham, Switzerland, 2018; Volume 25, pp. 233–282.
23. Gutteridge, W.; Dalziel, J. Filler cement: The effect of the secondary component on the hydration of Portland cement: Part 2: Fine hydraulic binders. *Cem. Concr. Res.* **1990**, *20*, 853–861. [CrossRef]
24. Marzouki, A.; Lecomte, A.; Beddey, A.; Diliberto, C.; Oueddou, M.B. The effect of grinding on the properties of Portland-limestone cement. *Const. Build. Mater.* **2013**, *48*, 1145–1155. [CrossRef]
25. Matschei, T.; Lothenbach, B.; Glasser, F.P. The Role of Calcium Carbonate in Cement Hydration. *Cem. Concr. Res.* **2007**, *37*, 551–558. [CrossRef]
26. Li, G. Properties of High-Volume Fly Ash Concrete Incorporating Nano-SiO₂. *Cem. Concr. Res.* **2004**, *34*, 1043–1049. [CrossRef]
27. Kirkpartick, R.J.; Yarger, J.L.; McMillan, P.F.; Yu, P.; Cong, X. Raman spectroscopy of C-S-H, tobermorite, and jennite. *Adv. Cem. Based Mater.* **1997**, *5*, 93–99. [CrossRef]

28. Garbev, K.; Stemmermann, P.; Black, L.; Breen, C.; Yarwood, J.; Gasharova, B. Structural features of C-S-H(I) and its carbonation in air-A Raman spectroscopic study. Part I: Fresh phases. *J. Am. Ceram. Soc.* **2007**, *90*, 900–907. [[CrossRef](#)]
29. Mohammad, W.A.S.B.W.; Othman, N.H.; Ibrahim, M.H.W.; Rahim, M.A.; Shahidan, S.; Rahman, R.A. A review on seashells ash as partial cement replacement. *IOP Conf. Ser. Mater. Sci. Eng.* **2017**, *271*, 012059. [[CrossRef](#)]
30. Wang, Z.; Chen, Y. Data-driven modeling of building thermal dynamics: Methodology and state of the art. *Energy Build.* **2019**, *203*, 109405. [[CrossRef](#)]
31. Lotteau, M.; Loubet, P.; Pousse, M.; Dufrasnes, E.; Sonnemann, G. Critical review of life cycle assessment (LCA) for the built environment at the neighborhood scale. *Build. Env.* **2015**, *93*, 165–178. [[CrossRef](#)]